Forensic seismic evidence for precursory mobilization in Gaza leading to the October 7 terrorist attack

A. Inbal, Department of Geophysics, Tel Aviv University, Tel Aviv, Israel

Declaration of Competing Interests

The authors acknowledge there are no conflicts of interest recorded.

Corresponding Author

Asaf Inbal, Department of Geophysics, Tel Aviv University, Tel Aviv, Israel, Email: asafinbal@tauex.tau.ac.il

Abstract

Seismic waves excited by human activity frequently mask signals due to tectonic processes, and are therefore discarded as nuisance. Seismic noise-field analysis is, however, a powerful tool for characterizing anthropogenic activities. Here, I apply this analysis to examine seismic precursors to the October 7 Hamas attack on Israel. The precursory activity in Gaza included massive mobilization which took place in the hours leading to the attack, and was documented on multiple media outlets. Favourable conditions, which arise due to a temporary lack of anthropogenic activity in Israel, allow remote seismic stations to record signals due to Gaza vehicle traffic. I use these seismograms in order to identify anomalous ground-motions, associate them with pre-attack mobilization, and precisely determine their location. By applying array analysis to three seismic stations located tens-of-kilometers from the Gaza strip, I was able to obtain valuable information on the Hamas attack plans. This suggests that embedding seismic noise-field analysis into decision-making protocols could enhance preparedness, thus providing an opportunity to blunt terrorist attacks and reduce the number of casualties.

Introduction

On October 7, 2023, 06:30 (local time), Hamas terrorists launched an unprecedented attack on southwestern Israel. Their operation initiated with a simultaneous breach of the barrier surrounding the Gaza strip, a densely populated area bordering southwest Israel, which is the locus of an on-going armed conflict between Israel and Palestine (Figure 1). The barrier breach was followed by a massive air-, land-, and sea-borne invasion of 2000-3000 Palestinians, who stormed Israeli near-border military camps, and then took-over rural and urban civilian centers. This assault, which took Israel by surprise, resulted in the killing of 1200 Israelis and an unknown number of Palestinians, and the kidnapping of 240 Israelis into Gaza. In response, Israel declared war on the Hamas, initiated heavy bombardment of Gaza, and invaded it from the ground.

Clearly, if warning had been issued, then the Israeli Defense Force (IDF) would have been able to blunt the attack. However, it appears that the whereabouts of Hamas militants during the hours preceding the attack were largely unknown. The barrier breach required thousands of troops be mobilized towards positions assumed along the Gaza barrier (Figure 1). This inference is supported by footage showcasing Palestinians riding light vehicles during the early hours of October 7 [e.g. *Swaine et al.*, 2023]. That traffic volume must have been unusually large relative to regular Saturdays pre-dawn traffic. The fact that despite heavy surveillance Hamas manged to surprise Israel, suggests their mobilization likely took place in the hours or minutes preceding the breach.

Thus, traffic-induced seismic waves generated due to forces imparted by vehicles traversing Gaza, were recorded by seismometers pertaining to the Israeli Seismic Network (IS). At a range of tens-of-kilometers, such traffic-induced seismic waves usually appear on broadband seismograms as emergent 2 to 8 Hz signals. Under favourable conditions, those signals may exceed the

background noise levels [*Inbal et al.*, 2018]. The Hamas' attack took place early on Saturday morning, on the eve of Simchat Tora, a national Jewish Holiday. Saturdays are off-work days in Israel, and therefore their early morning hours are characterized by very light traffic and no industrial activity. That October 7 was also a national holiday, ensures the IS stations background seismic noise levels were especially low. The low background noise levels on the one hand, and the anomalous mobilization in Gaza on the other hand, suggest the mobilization signal may have been recorded by some of the IS broadband stations, despite being located tens-of-kilometers from Gaza.

The objective of this report is two-fold. First, to examine whether precursory activity leading to the October 7 attack showed up on the IS stations. Second, to investigate whether these seismograms could have been used to issue warning of preparations for an immediate large-scale attack. It will be shown that multiple precursory arrivals during the hours leading to the attack locate to sources in the Gaza strip, and that these locations reveal important details on Hamas's attack plans.

Temporal and spectral analysis of the October 7 seismic noise field

Under favourable SNR conditions, traffic induced surface- and body-waves can sometimes show up on seismograms recorded tens-of-kilometers from the source. The number, speed, location, and mass of the Hamas' vehicles traveling in Gaza in the early hours of October 7 are unknown, making it impossible to estimate whether any pre-attack motions produced a signal exceeding the background noise level. Yet, visual inspection of IS network seismograms reveals signals exceeding the noise levels at the stations nearest to the Gaza strip during the two hours before the attack. Seismograms and spectra recorded on the day of the attack at IS stations AMZNI, YATR, and KZIT are shown in Figure 2. Each of the spectra exhibit a clear peak that rises

above the background noise level, which was estimated from Saturdays during 2021, 2022, and 2023 for the time window encompassing the pre-attack spectra. The highest signal-to-noise ratio (SNR) for AMZNI, YATR, and KZIT is observed at frequencies ranging between 2.1 to 2.8 Hz, 5.5 to 6.5 Hz, and 2.8 to 3.2 Hz, respectively, and are referred to here as the target frequency bands. Seismic signals in these frequency bands had previously been associated with traffic activity [*Yamanaka et al.*, 1993; *Bonnefoy-Claudet et al.*, 2006; *Groos and Ritter*, 2009; *Riahi and Gerstoft*, 2015; *Inbal et al.*, 2018; *Mi et al.*, 2022]. Interestingly, the three spectral peaks, which presumably originated from a common source (or sources), do not overlap. Similar behavior had previously been observed for ground motion modulated by remote wind-turbine activity [*Inbal et al.*, 2018], and may be the result of variability of the thicknesses of the upper layer encountered along the path to the stations. To qualitatively assess these effects, I have used a discrete wavenumber reflectivity method [*Cotton and Coutant*, 1997] to calculate synthetic spectra excited by a vertical force acting on the surface of a plane-layered model consisting of a low-velocity thin layer overlaying a homogeneous uniform elastic half-space. The spectra computed for upper-layer thicknesses of 10 and 100 m (Figure 3 ; see table S1 for the layer properties), consistent with the width of the upper soft sedimentary layer in the study area [*Gardosh et al.*, 2011], peak at frequencies close to the ones observed to peak in the IS data. Other factors that can affect the spectra include the spatial distribution of sources, whose extent is close to the aperture of the IS stations, the local topography, and the depth to the water table.

The IS seismograms are analyzed after applying a 4th order Butterworth filter in the three target frequency bands. Visual inspection reveals distinct amplitude fluctuations appearing from about 20 minutes before the attack (Figure 2a), which can be observed on all three stations after averaging their Fourier amplitude spectra in the target frequency bands (Figure 4a-c). The

amplitude fluctuations are most well observed at YATR, the quietest of the three stations. YATR records a sequence of 5 strong bursts, each lasting for about 30 to 60 seconds. The first burst, occurring at about 06:15:30, and the last burst, occurring at about 06:29:30, exceed the noise levels of all three stations.

Given the large inter-station separation and the time-frequency attributes of the pre-attack signals, any correlation among the three stations would require waves induced by a large traffic source (in volume or mass). Because the traffic in Israel on the morning of October 7 (or other Saturday mornings prior to October 7, 2023 ; see below) was too sparse to give rise to correlated signals at the station triplet, inter-station seismic correlation is a strong indication that the signal observed on the IS stations is related to motions inside Gaza. To identify this correlation, I computed the three-component-averaged spectral amplitude for 30-second-long windows during the hours leading to the attack. The Fourier spectral amplitude were averaged over the three target frequency bands shown in Figure 2a-c. These time-series are indicated by the black curves in Figure 4. The background noise amplitudes computed from Saturday mornings between 2021 and 2023 are indicated by the grey curves, and their median value by the blue curves. The October 7 data show a sharp increase starting at about 06:10 local time, 20 minutes before the attack, especially at YATR and AMZNI. The seismic energy increase during the 20 minutes preceding the attack is substantial, averaging to about 150% the median background level, with multiple windows in YATR and KZIT carrying energy of up to 200% the median background signal energy level.

I used the background noise levels to estimate the likelihood random fluctuations in the target frequency bands may have coincided at all three stations. To test for significance I generated 10^6 1500-second-long time-series whose number of samples equals that of the observed time-

series at each station. The random amplitudes follow a normal distribution whose mean and standard deviation are extracted from the background noise curves. I count the number of windows exceeding 150% the background median, which is approximately the mean amplitude level observed during the last 1500 s before the attack, and the distribution of the average amplitude correlation-coefficient for the random realizations obtained for each station pair (Figure S1). The tests suggest that the probability the amplitude of three random 1500-second-long signals (drawn from distributions characteristic of the background noise), will rise once or twice above 150% of the median pre-attack background level is 5% and 0.03%, respectively (Figure S1b and S1c). In reality, however, amplitudes during the 1500 s preceding the attack reached >150% of the median background levels during multiple 30-s windows in all three stations, establishing the statistical significance of the October 7 observations at a high level of confidence.

Further indication to the strong October 7 inter-station correlation is shown in panels 4d-f, which present the amplitude covariation in the 20 minutes leading to the attack. The degree to which the October 7 correlation stands out above the background correlations is remarkable. For example, the pair AMZNI-YATR correlates at 92% at the day of the attack, but averages to only 10% during the previous Saturday mornings. The October 7 data at the other two station pairs are slightly less well-correlated, yet their pre-attack correlation level far exceeds the one expected given the correlation observed in the preceding Saturdays. The statistical analysis suggests $< 10^{-6}$ probability the average of the station pairs background amplitudes would correlate at >85% (Figure S1a), as was observed on October 7.

The synthetic tests were conducted assuming the amplitudes are distributed as during previous Saturdays and in the target frequency bands observed on October 7. Because diurnal, weekly, and annual variations in the spectral shapes are common, it is important to estimate whether

the strong correlations observed on October 7 (Figure 4d-f) can be observed on other days but at different frequency bands. This likelihood is estimated by selecting the 2 to 8 Hz spectral maxima after smoothing the spectra using a 1 Hz window (close to the widths of the October 7 spectral bumps ; Figure 2), and correlating the amplitudes recorded between 06:10 and 06:30 local time Saturdays starting from March, 2021. The average AMZNI-KZIT, AMZNI-YATR, and KZIT-YATR correlations coefficients are 0.09±0.46, 0.05±0.46, and 0.14±0.41, respectively. These values are significantly smaller than the October 7 correlations. Moreover, in only 8 of the preceding 143 Saturdays did the average correlations lie between 0.6 and 0.7, however these days do not exhibit the October 7, 2023, high amplitude level and almost-monotonic increase with time towards the attack (Figure 4a-c). This rules out the possibility that the October 7 correlations had emerged by chance.

Gaza traffic source location from tripartite array analysis

Seismograms from the station triplet may be used to locate sources giving rise to coherent surface waves travelling outwards from the Gaza strip, for example due to ground impacts produced by heavy vehicles. These coherent events were located from tripartite array analysis applied to the three IS stations. The IS seismograms are first band-pass filtered between 2 to 6 Hz and downsampled to a rate of 40 samples-per-second. Then, the vertical channel time delays are obtained by cross-correlating a sliding 30-second window with 50% overlap starting from 8000 s before the attack. For each candidate window at one station, I examine windows from a second station over intervals ranging from $-T_r$ to T_r, where T_r is the inter-station surface wave travel time, assuming the wave travels at 1.5 km/s. I then shift the horizontal channels at one station by the time-delay corresponding to the maximum vertical cross-correlation. Next, I search for the pair of rotations maximizing the horizontal channel cross-correlations. I rotate the two pairs

of horizontal seismograms at 10° intervals over a range of possible angles. Because rotating by more than 180° causes the polarity to flip, one channel pair is restricted to rotate between 0 to 180°, whereas the other pair is rotated between 0 to 360°. The technique is similar to one that was previously applied in order to enhance catalogs of weak and emergent seismic signals attributed to tectonic tremors in Cascadia [*Armbruster et al.*, 2014] and Mexico [*Peng and Rubin*, 2017]. Similar to traffic induced noise, tectonic tremors give rise to signals containing multiple repeated narrow-band wavelets [*Shelly et al.*, 2007; *Inbal et al.*, 2018], which sometimes facilitate correlating seismograms recorded by stations distant from each other.

For perfectly coherent arrivals, the sums of three time delays and the three rotation angles equal zero. Thus, the observed sums can be used to assess the detection quality. The tripartite array self-consistency criteria are defined as [*Eisermann et al.*, 2018]:

$$Q_{\Delta t} = 1 - \frac{\Delta t_{12} + \Delta t_{23} - \Delta t_{13}}{|\Delta t_{12}| + |\Delta t_{23}| + |\Delta t_{13}|}$$
$$Q_{\Delta \theta} = 1 - \frac{\Delta \theta_{12} + \Delta \theta_{23} - \Delta \theta_{13}}{|\Delta \theta_{12}| + |\Delta \theta_{23}| + |\Delta \theta_{13}|} \quad (1)$$

,

where Δt_{ij} and $\Delta \theta_{ij}$ are the time-delay and relative rotation between station j to station i, respectively. For high-quality detections, $Q_{\Delta t}$ and $Q_{\Delta \theta}$ are approximately equal to 1. To ensure the robustness of the locations, I retain time windows with $Q_{\Delta t}$ and $Q_{\Delta \theta}$ larger than 0.7, which amounts to about 10% of the total number of windows.

The time-delay measurements passing the self-consistency criteria are used for determining the source locations via a grid-search approach. The difference between the distance from the i'th station to source to the distance from the j'th station to the source can be written as a function of the product between the wave speed and the observed time-delay:

$$R_j - R_i = c\Delta t_{ij}, \quad (2)$$

where $R_j = ||\mathbf{x_j^r} - \mathbf{x^s}||_2$, and $\mathbf{x^s}$ and $\mathbf{x_j^r}$ are vectors holding the surface coordinates of the source and the j'th station, respectively. I solve for a uniform surface wave speed and for the surface location along the Salah Al-Deen Road, a major traffic artery crossing the Gaza strip from Rafah in the south to Beit Lahia in the north (Figure 1 and 5). To find the best-fit wave-speed c and source location $\mathbf{x^s}$, I set $i = 1$ and perform a grid search over $\mathbf{x^s}$, restricting the search for locations along the Salah Al-Deen Road, and for c in the range between 0.6 to 3 km/s. I retain locations for which the misfit between the two observed and two calculated time-delays is smaller than 1 second (see inset histogram in Figure 5). These correspond to errors that are of the order of 2-3% of the source-to-receiver travel-times. Figure S2 presents an example of a misfit function for one detection, and the distribution of wave-speeds obtained from this analysis. The average wave speed is 1.1±0.3 km/s. To validate the wave speeds obtained via optimization, I compare them to speed of surface waves excited by known impacts (Figure S4), which give speeds between 1 and 1.8 km, slightly higher than the speeds recovered from minimizing Equation 2. This may be due to harder sedimentary rocks found between station YATR to JER and RMNI relative to the softer rocks typical of the coastal planes found between the Gaza strip and stations AMAZIN, YATR, and KZIT.

The location resolution is obtained by analyzing the Equal Differential Travel Time curves (EDT ; *Eisermann et al.* [2015]). In a uniform velocity model, the EDTs for each station pair are defined by hyperbolas that intersect at the source location, and whose width is determined by the uncertainties on the time-delay and velocity model. I assess the location resolution by perturbing the EDT curves according to the time-delay errors (estimated from the misfit distribution ; Figure 5 panel a) and wave speed range (estimated from the optimization results ;

Figure S2). The resolution for sources lying along the Salah Al-Deen Road is found to be about 1 km in the along-road direction, and about 12 km in the oblique direction (Figure S3).

The optimal rotation angles in windows passing the detection criteria were used to infer the horizontal motion polarization orientation, and to constrain the surface source locations. For Rayleigh and Love surface waves, the horizontal polarization angles are aligned in the radial and transverse directions, respectively. Hence the motions excited by the passing wave are dependent on the azimuth of the vector pointing from the station to the source, commonly referred to as the back-azimuth. For coherent arrivals, the back-azimuths from the three IS stations are expected to intersect at the source location. Thus, the polarization-derived back-azimuths may be used to determine source locations independently from the locations derived based on the time-delay measurements.

A map showing the pre-attack signal locations and optimal rotation angles is presented in Figure 5. Most of the sources are found to originate from a portion of the road extending between the city of Khan Younes in the south out towards the Al Zawayda and Nuseirat refugee camps, which are located just south of the City of Gaza. Fewer locations are resolved in the northern and southern most extents of the strip, near Beit Lahia and Rafah. These locations are compared with the locations inferred from the range of back-azimuth intersections. The intersection of the range of back-azimuths pointing from each of the stations defines a polygon centered on the Gaza strip, encompassing locations that were independently derived from correlation-based time-delay measurements. This consistency lends further support to the array-based location approach. At stations AMZNI and YATR the polarization directions are $0\pm30^\circ$ and $80\pm40^\circ$, respectively, and at KZIT it is $280\pm25^\circ$. Based on this observation, it is inferred that the AMZNI and KZIT

stations are mostly sensitive to Love waves, whereas the YATR station is mostly sensitive to Rayleigh wave energy.

The array analysis is applied to successive time windows, providing an opportunity to assess the space-time distribution of sources lying along the Salah Al-Deen Road. A time-series of the along-road locations during the last two hours before the attack began is presented in Figure 5b. Based on its space-time distribution, the activity can be grouped into two main phases, termed here the early and late Hamas deployments. During both phases, activity appears to have originated from Khan Younes and to advance mostly north towards the city of Gaza, and later towards Beit Lahia. The first deployment is associated with slightly slower motion, whose exact speed is difficult to determine given the scattered locations. A line connecting the first detections occurring after 04:45 in each portion of the Salah Al-Deen Road gives a minimal velocity of 44 km/s, which is indicated in panel 5b. The later detections in that phase may be associated with motions in the road-oblique direction.

The early phase consisted of activity that lasted for about an hour, and that was concentrated near Khan Younes and Al Zawayda. Between 05:45 to about 06:00, the rate of activity was diminished. Then, the activity resumed with fast advancement from Khan Younes north towards Beit Lahia and south towards Rahaf. The second deployment persisted for about 30 minutes, until 06:30 when the attack began. The two phases identified in the time-space plot in Figure 5b correspond to intervals in the IS seismograms containing high-amplitude seismic energy. The early deployment, which occurred between 04:45 to 05:45, is best observed on AMZNI and, to a lesser degree, also on KZIT (Figure 4a,c). The late deployment, between about 06:00 to 06:30, is manifested by an almost-monotonically increasing amplitude observed on the three stations during the minutes preceding the attack (Figure 4).

To assess the significance of the October 7 event location results, I applied the tripartite array location scheme to 100 1-hour-long time windows occurring on Friday nights and early Saturday mornings local time. By applying the same detection criteria used for the October 7 data to the 100 control windows, I find a regular hourly detection rate of approximately 5 events-per-hour. This rate is about 5 times lower than the one observed during the last 2 hours before the attack. Thus, the spatio-temporal distribution of coherent events presented in this section, and the seismic noise amplitudes evolution with lead time presented in the previous section, are the seismic signatures of precursory activity leading to the October 7 terrorist attack.

Discussion

How early could a seismic-based pre-attack warning been issued?

That seismic signal signal, attributed here to the late Hamas deployment in the Gaza strip, stands well-above the noise level, and is correlated at 85%-92% between the three station pairs. The strong pre-attack signal was preceded by a phase characterized by high-amplitude seismic energy, which lasted between 04:30 to 05:45 local time, and that was mostly observed at AMZNI, and to a lesser degree also at KZIT. Over such durations, one or two random signals are likely to rise to the observed levels. Thus, the signal observed at AMZNI and KZIT starting from 04:30, was hardly sufficient to confidently establish that anomalous activity was taking place in the Gaza strip. The probability for abnormal activity in Gaza significantly increased with the onset of the signal of the late Hamas deployment, from about 06:10. Given the background noise levels, the amplitudes observed between about 06:10 to 06:30 were sufficient to establish that large-scale mobilization was taking place within the Gaza strip at a high level of confidence. Starting from the onset of the second deployment, the level of confidence increased almost monotonically with

countdown to attack, finally reaching >99% in the last few minutes before the barrier breach began.

The results suggest that embedding analysis of traffic-induced seismic noise into decision-making protocols may be useful for detecting large-scale mobilization in real-time. Most seismic-based traffic detection systems rely on near-target recordings [e.g. *Bin et al.*, 2021], however analysis of the October 7 dataset suggests that, in certain conditions, remote stations could also be used for these purposes. Deploying stations further from the target area also means the network is less likely to be decapitated during the attack, as was the fate of many of the IDF near-fence systems on October 7. Since the type and origin of signals excited by pre-attack motions are not well characterized, monitoring areas as large as the Gaza strip would likely require a dense network. Such systems could provide tens-of-minutes lead time, which are crucial for preventing terrorist attacks, and for notifying nearby civilian communities.

Implications for Hamas pre-attack preparations

The space-time distribution of signals associated with anomalous traffic in Gaza (Figure 5b) bears important implications for the Hamas operational plan. The locations indicate that pre-attack mobilization originated near Khan Younes, a city believed to serve as a hideout for the senior Hamas leadership as well as for many of its troops, and where intense fighting is currently taking place [*Yazbek et al.*, 2023]. It is therefore not surprising to find prominent pre-attack activity in that area.

The timing and location of the most coherent signals support a two-stage deployment scheme. The early stage, which took place between 04:45 to 05:45 local time, consisted of slower, possibly sparser movement of troops north and south of Khan Younes. The activity extends out to about 15 km north of the city, and a few kilometers to its south. The troops likely paused between

05:45 to about 06:00, as is manifested by a decline in seismic amplitudes (Figure 4a-c), and, accordingly, in the rate of array-based detections (Figure 5b). One possibility is that in this lag, troops advanced and then paused to watch for activity in Israel suggesting their earlier motions have been detected. This scenario is consistent with IDF reports of the last pre-attack near-barrier activity taking place northeast of Nuseirat at about 05:00 local time. The location of that near-barrier activity is in agreement with locations of coherent arrivals resolved by the IS stations, and lack of later pre-attack reports is consistent with the inter-deployment seismic quiescence.

The duration of the no-detection epoch suggests Hamas militants took about 15 minutes to confirm the IDF hadn't spotted their advancement. The ensuing detection rate and amplitude increase suggest that the pause was followed by a rapid and larger wave of troops who left the Khan Younis area and spread out towards the furthest extent of the Gaza strip. It seems that once the second wave reached Beit Lahia and Rafah, in the northern and southern most edges of the strip, an order was given to hit all near-barrier positions at once.

Acknowledgments. A. Ziv initially proposed to search for the precursory seismic signal. J.-P. Ampuero commented on an early version of this manuscript. This research was conducted while I was on leave at Université Côte d'Azur, Nice, France, enabled through a generous grant provided by the Observatoire de la Côte d'Azur. The work is dedicated to the victims of the October 7 terrorist attack.

Data and Resources. Data from the IS network are available from https://seis.gsi.gov.il/fdsnws.

References

Armbruster, J. G., W.-Y. Kim, and A. M. Rubin (2014), Accurate tremor locations from coherent S and P waves, *J. Geophys. Res.*, *119*(6), 5000–5013, doi:10.1002/2014JB011133.

Bin, K., J. Lin, X. Tong, X. Zhang, J. Wang, and S. Luo (2021), Moving target recognition with seismic sensing: A review, *Measurement*, *181*, 109,584, doi: https://doi.org/10.1016/j.measurement.2021.109584.

Bonnefoy-Claudet, S., F. Cotton, and P.-Y. Bard (2006), The nature of noise wavefield and its applications for site effects studies: A literature review, *Earth-Science Reviews*, *79*, 205–227, doi:10.1016/j.earscirev.2006.07.004.

Cotton, F., and O. Coutant (1997), Dynamic stress variations due to shear faults in a plane-layered medium, *Geophys. J. Int.*, *128*(3), 676–688, doi:10.1111/j.1365-246X.1997.tb05328.x.

Eisermann, A. S., A. Ziv, and G. H. Wust-Bloch (2015), Real-Time Back Azimuth for Earthquake Early Warning, *Bull. Seismo. Soc. Am.*, *105*(4), 2274–2285, doi:10.1785/0120140298.

Eisermann, A. S., A. Ziv, and H. G. Wust-Bloch (2018), Array-Based Earthquake Location for Regional Earthquake Early Warning: Case Studies from the Dead Sea Transform, *Bull. Seismo. Soc. Am.*, *108*(4), 2046–2053, doi:10.1785/0120170315.

Gardosh, M., P. Weimer, and A. Flexer (2011), The sequence stratigraphy of Mesozoic successions in the Levant margin, southwestern Israel: A model for the evolution of southern Tethys margins, *AAPG Bulletin*, *95*(10), 1763–1793, doi:10.1306/02081109135.

Groos, J. C., and J. R. R. Ritter (2009), Time domain classification and quantification of seismic noise in an urban environment, *Geophy. J. Int.*, *179*(2), 1213–1231, doi:10.1111/j.1365-246X.2009.04343.x.

Inbal, A., T. Cristea-Platon, J. Ampuero, G. Hillers, D. Agnew, and S. E. Hough (2018), Sources of Long-Range Anthropogenic Noise in Southern California and Implications for Tectonic Tremor Detection, *Bull. Seismo. Soc. Am.*, *108*(6), 3511–3527, doi:10.1785/0120180130.

Mi, B., J. Xia, G. Tian, Z. Shi, H. Xing, X. Chang, C. Xi, Y. Liu, L. Ning, T. Dai, J. Pang, X. Chen, C. Zhou, and H. Zhang (2022), Near-surface imaging from traffic-induced surface waves with dense linear arrays: An application in the urban area of Hangzhou, China, *Geophys.*, *87*(2), B145–B158, doi:10.1190/geo2021-0184.1.

Peng, Y., and A. M. Rubin (2017), Intermittent tremor migrations beneath Guerrero, Mexico, and implications for fault healing within the slow slip zone, *Geophys. Res. Lett.*, *44*(2), 760–770, doi:10.1002/2016GL071614.

Riahi, N., and P. Gerstoft (2015), The seismic traffic footprint: Tracking trains, aircraft, and cars seismically, *Geophys. Res. Lett.*, *42*(8), 2674–2681, doi:10.1002/2015GL063558.

Shelly, D. R., G. C. Beroza, and S. Ide (2007), Non-volcanic tremor and low-frequency earthquake swarms, *Nature*, *446*(7133), 305–307, doi:10.1038/nature05666.

Swaine, J., L. J. Sohyun, S. Cahlan, I. Piper, B. Monroe, E. Hill, and M. Kelly (2023), How Hamas exploited Israel's reliance on tech to breach barrier on Oct. 7, The Washington Post, accessed: 2023-12-05.

Yamanaka, H., M. Dravinski, and H. Kagami (1993), Continuous measurements of microtremors on sediments and basement in los angeles, california, *Bull. Seismo. Soc. Am.*, *83*(5), 1595–1609.

Yazbek, H., C. Koetti, and M. Levenson (2023), Israeli Forces Near Major City in Southern Gaza as Civilians Panic, The New York Times, accessed: 2023-12-05.

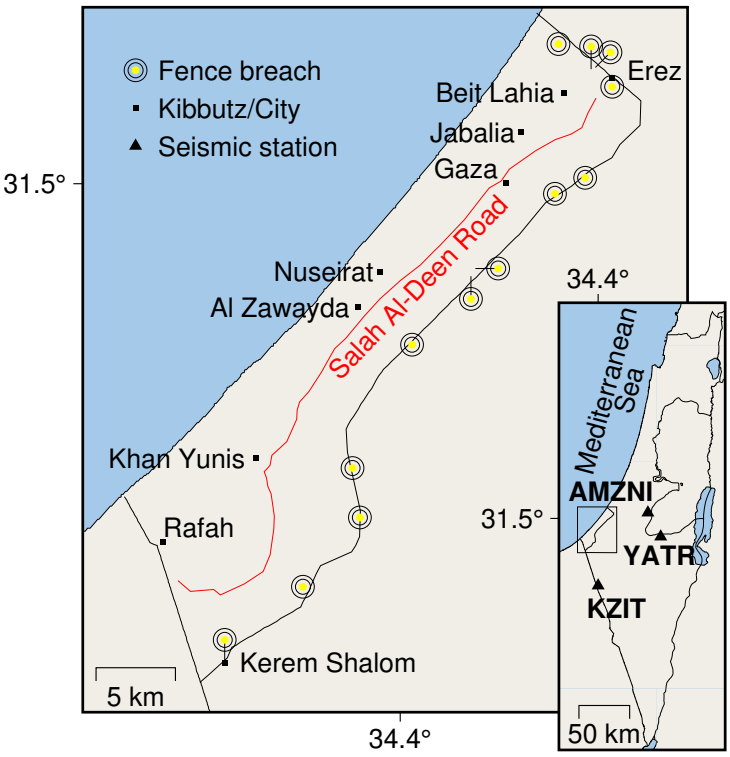

Figure 1. Location map showing the Gaza strip and the surrounding area. Yellow circles indicate location of fence breaches reported on October 7, 2023. Black squares are for the Palestinian cities and of Beit Lahia, Jabalia, Gaza, Nuseirat, Al Zawayda, Khan Younes, and Rafah, and the Israeli Kibbutzim Erez and Kerem Shalom. Inset shows the location of AMZNI, YATR, and KZIT, the three seismic stations used in this study. The Salah Al-Deen Road is indicated by the red curve, and international borders are indicated by the black curves.

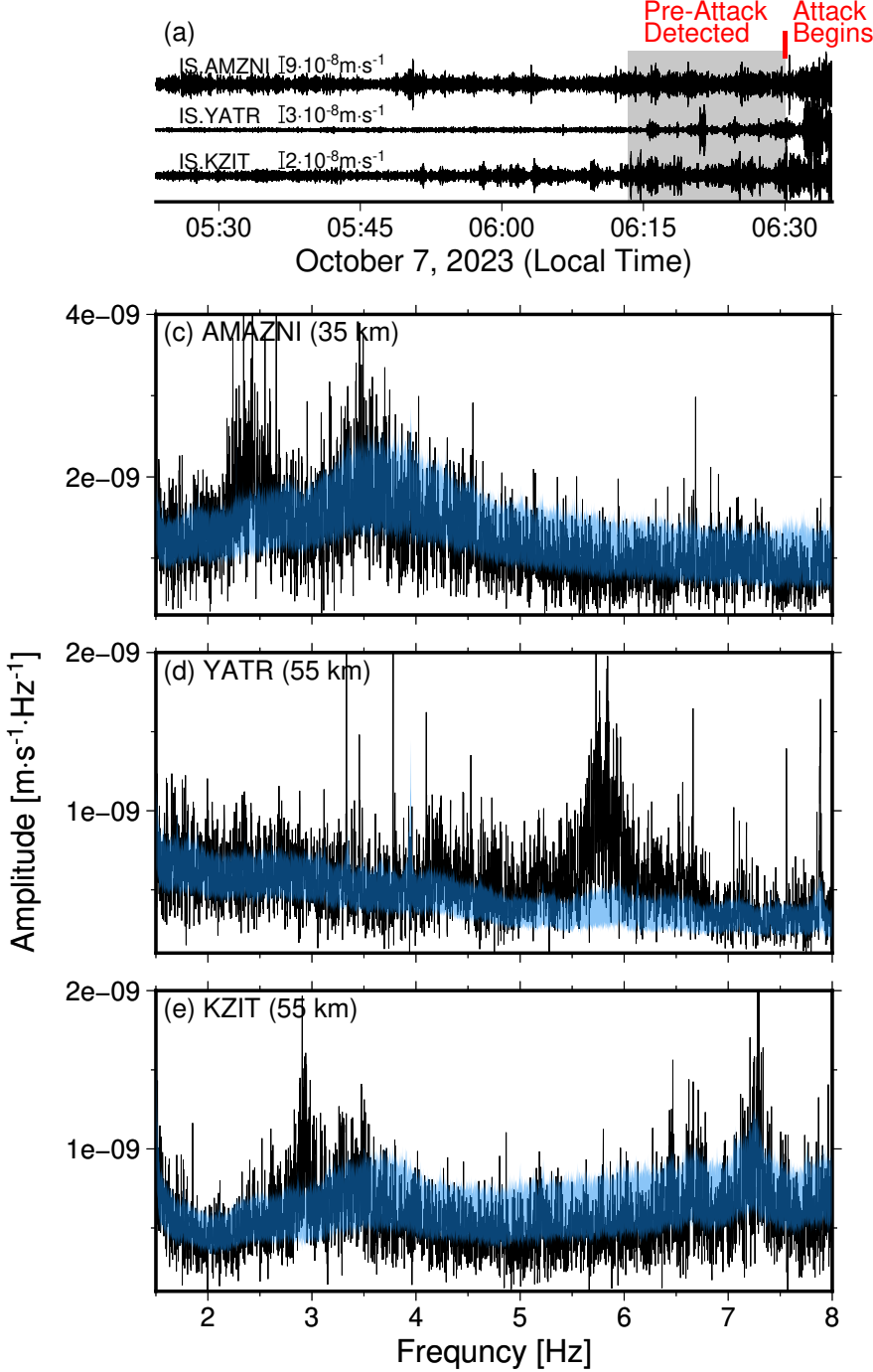
(a)
Pre-Attack Detected
Attack Begins
IS.AMZNI
IS.YATR
IS.KZIT
05:30
05:45
06:00
06:15
06:30
October 7, 2023 (Local Time)
(c) AMAZNI (35 km)
(d) YATR (55 km)
(e) KZIT (55 km)
4e−09
2e−09
1e−09
Amplitude [m·s⁻¹·Hz⁻¹]
2
3
4
5
6
7
8
Frequncy [Hz]

Figure 2. The seismograms and spectra from the three IS stations recording the seismic precursor on the morning of October 7. The attack began at 06:30 local time. (a) Vertical component seismograms from AMZNI, YATR, and KZIT showing ground velocity as a function of local time on October 7. The grey rectangle indicates the portion of the pre-attack seismograms where strong correlated signals are observed on YATR and KZIT. Note that strong noise fluctuations begin at AMZNI around 05:10 (Figure 4a), before the earliest time shown in this panel. (b-d) Three-component spectra recorded at AMZNI, YATR, and KZIT. The black curve is for the time window between 06:20 and 06:30 on October 7. The light-blue strip shows the median background noise level $\pm$ 1 median standard deviation. The noise curve was computed from spectra recorded during Saturday mornings between 2021 and 2023.

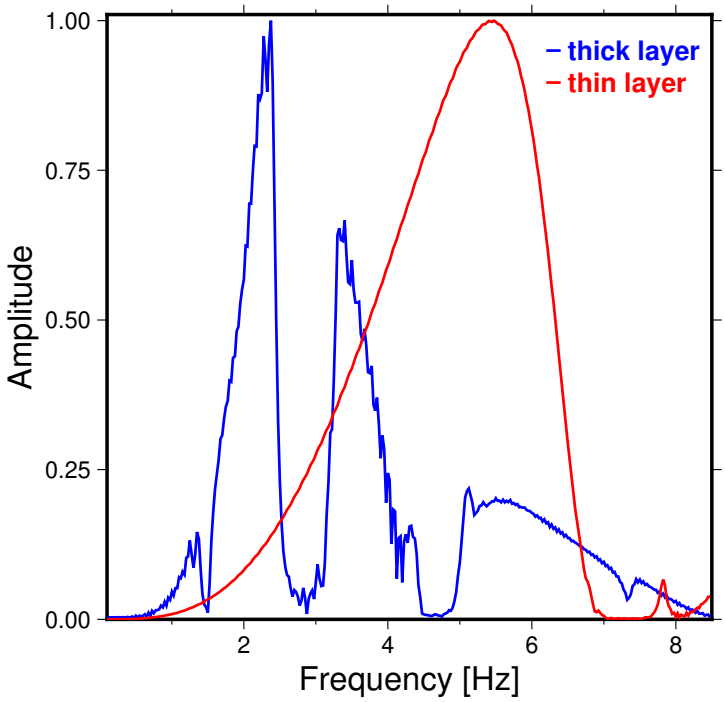

Figure 3. Synthetic three-component-averaged ground velocity spectra for a vertical force acting on the surface of a two-layer model. The red and blue curves indicate spectra computed for two-layer models whose upper layer thickness is 20 and 100 m, respectively. The receivers are located at epicentral ranges of 50 to 60 km, approximately the ones between the IS stations and Gaza. Spectra are normalized by their maxima.

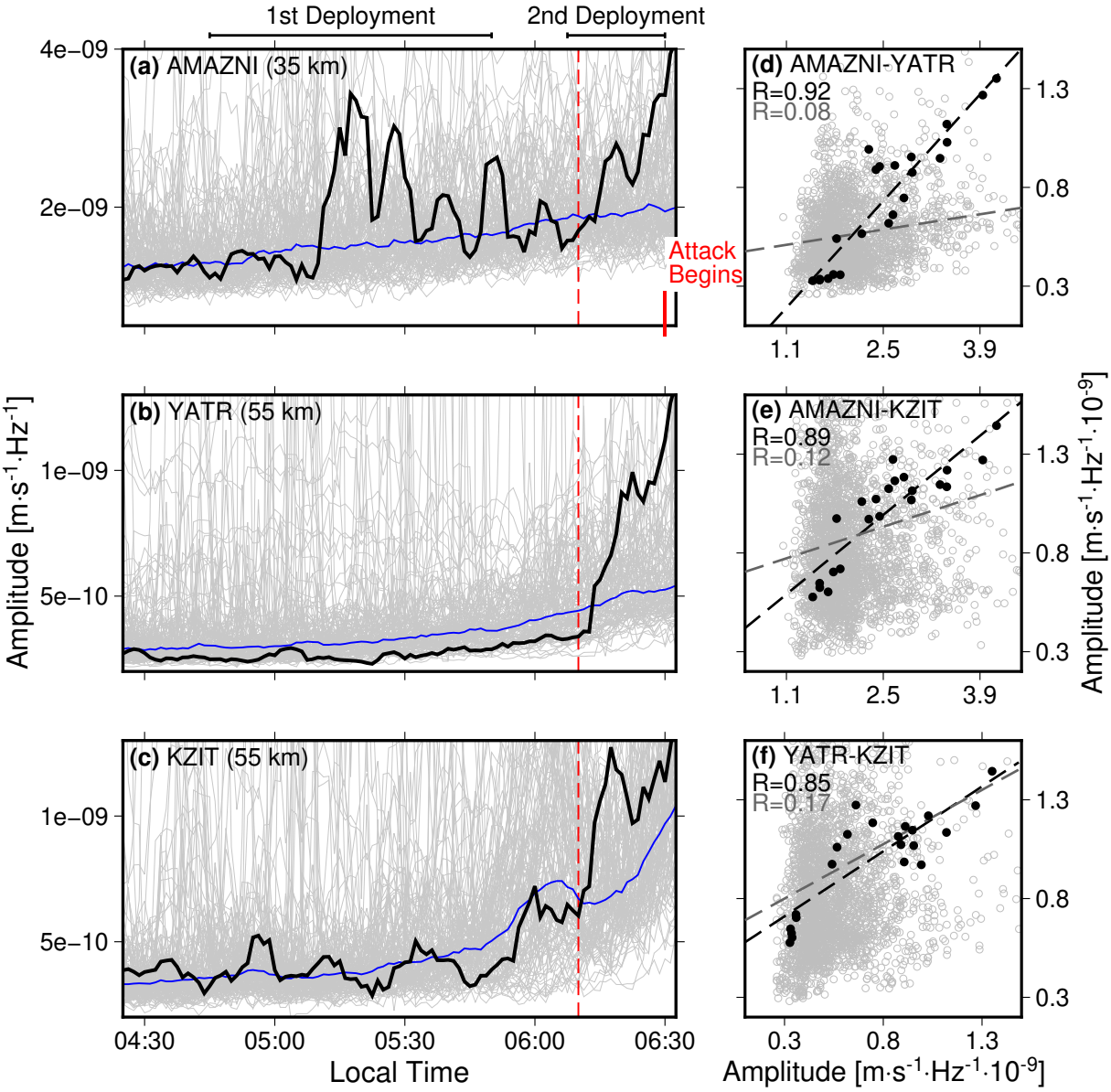
1st Deployment
2nd Deployment
(a) AMAZNI (35 km)
(b) YATR (55 km)
(c) KZIT (55 km)
Attack Begins
Amplitude [m·s-1·Hz-1]
Local Time
04:30
05:00
05:30
06:00
06:30
(d) AMAZNI-YATR
R=0.92
R=0.08
(e) AMAZNI-KZIT
R=0.89
R=0.12
(f) YATR-KZIT
R=0.85
R=0.17
Amplitude [m·s-1·Hz-1·10-9]

Figure 4. Pre-attack seismic amplitudes as a function of time, and the seismic amplitude inter-station correlation. The progression of seismic amplitudes at three IS seismic stations during the 2 hours leading to the attack are shown in the left column, and the covariation of amplitudes during the last 30 minutes before the attack are shown in the right column. (a-c) The three-component averaged spectral amplitudes as a function of local time on October 7 are shown by the black curves. The AMZNI, YATR, and KZIT amplitude curves are computed by averaging over frequencies between 2.1 to 2.8 Hz, 5.5 to 6.3 Hz, and 2.7 to 3.3 Hz, respectively. The background noise curves in these frequency bands and their median are shown by the grey and blue curves, respectively. The red dashed curve indicates the initiation of the 2nd deployment stage, characterized by high amplitude seismic energy and strong inter-station correlations. The amplitudes were computed for successive 300-second long windows with 75% overlap. (d-f) Amplitude covariation during the 2nd deployment stage, starting from 06:10 local time. Each panel shows the October 7 and background amplitudes in one station plotted against the amplitudes at another station. The station pair used for each panel is shown in the upper left corner. Dashed black and grey curves indicate linear fits to the data. The value of R, the correlation between the linear fit and the observations, is given in black for the pre-attack window, and in grey for the mean of the curves fitted for the windows covering the preceding Saturdays during 2021, 2022, and 2023.

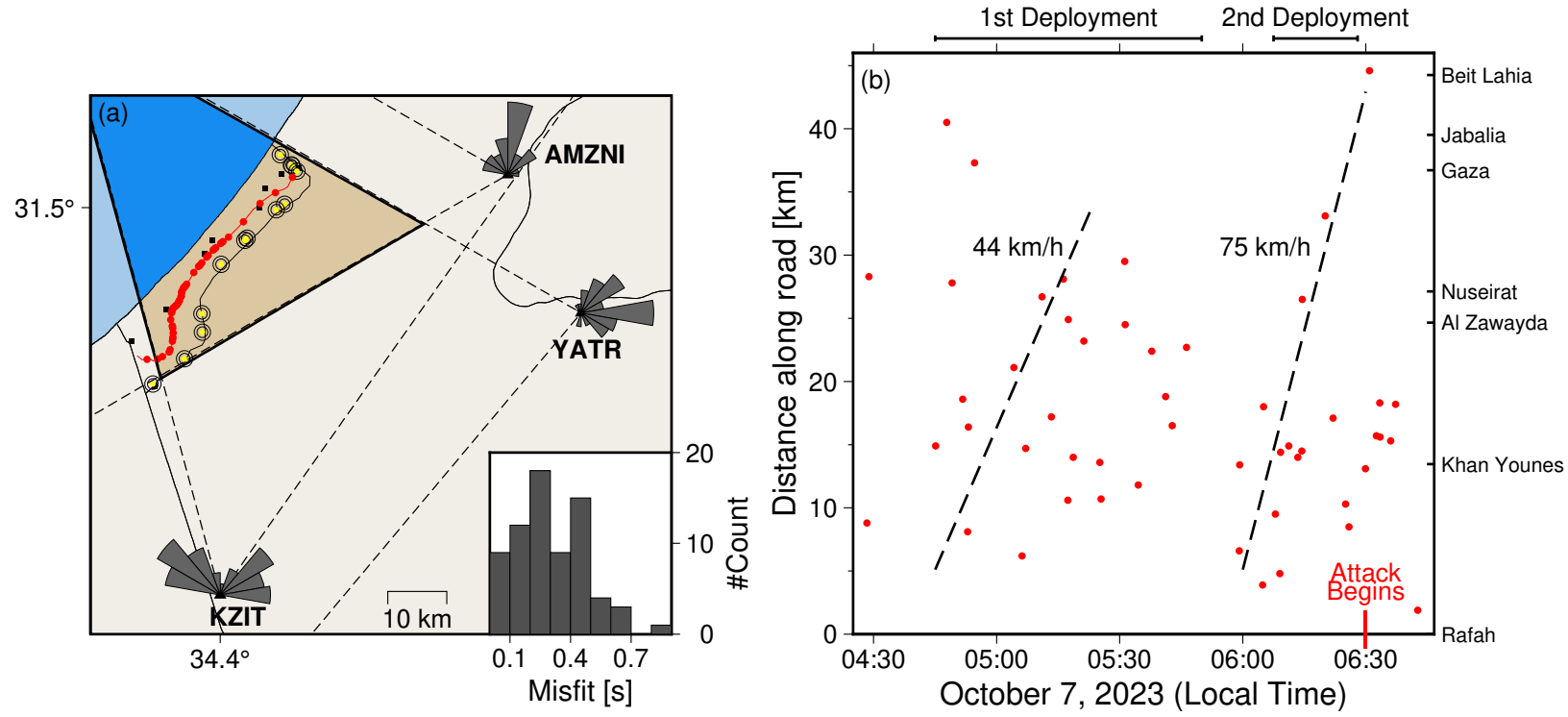

Figure 5. Tripartite array analysis results. (a) The location of coherent seismic bursts along the Salah Al-Deen Road observed during the two hours preceding the attack are shown by the red circles. Note that the location assumes sources are located along the portion of the road marked by the red line in the figure. The polar diagrams show the distribution of rotation angles at each station. Dashed lines indicate the range of back-azimuths resolved at each station, and the highlighted polygon indicates the area formed by the back-azimuth intersection. The barrier breaches are indicated by the yellow circles, and local Palestinian towns and Israeli Kibbutzim are indicated by the black squares. The inset histogram presents the distribution of the misfit between the observed and calculated surface waves travel-times. (b) Space-time analysis of coherent seismic bursts located along the Salah Al-Deen Road. Dashed lines denote constant velocities of 44 and 75 km/s. The right vertical axis indicates location of Palestinian towns along the Salah Al-Deen Road.